coatings

MDPI

Article

Boosting the Visible Light Photocatalytic Activity of ZnO through the Incorporation of N-Doped for Wastewater Treatment

Md. Abu Hanif [1,*], Young Soon Kim [1], Sadia Ameen [2], Hong Gun Kim [1,3] and Lee Ku Kwac [1,3,*]

[1] Institute of Carbon Technology, Jeonju University, Jeonju 55069, Korea; kyscjb@jj.ac.kr (Y.S.K.); hkim@jj.ac.kr (H.G.K.)
[2] Materials and Devices Laboratory, Department of Bio-Convergence Science, Advanced Science Campus, Jeonbuk National University, Jeongeup 56212, Korea; sadiaameen@jbnu.ac.kr
[3] Graduate School of Carbon Convergence Engineering, Jeonju University, Jeonju 55069, Korea
* Correspondence: hanif21@jj.ac.kr (M.A.H.); kwac29@jj.ac.kr (L.K.K.); Tel.: +82-63-220-3157 (M.A.H.); +82-63-220-3063 (L.K.K.)

Abstract: In the present work, we prepared N-doped ZnO by a facile chemical vapor deposition method and used it for the degradation of wastewater containing noxious rose bengal (RB) dye under visible-light stimulation. The as-prepared N-doped ZnO and the undoped ZnO (used as a control sample) were characterized by numerous spectroscopic and microscopic methods. These analyzing results confirmed the successful formation of the N-doped ZnO compound and it could be implemented for wastewater treatment. Interestingly, the N-doped ZnO material confirmed the maximum RB dye degradation efficiency (96.90%) and was shown to be 154% more efficient than undoped ZnO (62.95%) within 100 min of visible-light irradiation. The bandgap energy was considerably decreased after the incorporation of N onto the ZnO matrix compared to undoped ZnO. The improved photocatalytic performance is because of the reduction of bandgap energy, which suppressed the electron–hole pair recombination. In addition, a plausible photodegradation mechanism of RB dye was discussed employing N-doped ZnO under visible light. The findings show that our as-synthesized product can be used to eliminate contaminants, which provides a new avenue for effective implications.

Keywords: N-doped ZnO; chemical vapor deposition; rose bengal dye; bandgap energy; wastewater treatment

check for updates

Citation: Hanif, M.A.; Kim, Y.S.; Ameen, S.; Kim, H.G.; Kwac, L.K. Boosting the Visible Light Photocatalytic Activity of ZnO through the Incorporation of N-Doped for Wastewater Treatment. *Coatings* **2022**, *12*, 579. https://doi.org/10.3390/coatings12050579

Academic Editor: Joaquim Carneiro

Received: 25 March 2022
Accepted: 21 April 2022
Published: 24 April 2022

Publisher's Note: MDPI stays neutral with regard to jurisdictional claims in published maps and institutional affiliations.

Copyright: © 2022 by the authors. Licensee MDPI, Basel, Switzerland. This article is an open access article distributed under the terms and conditions of the Creative Commons Attribution (CC BY) license (https://creativecommons.org/licenses/by/4.0/).

1. Introduction

Air, water, and soil contamination are the three major classes of environmental pollution. Water pollution is one of them, and it is becoming worse every day for a variety of reasons [1]. The current epoch is known as the industrial revolution. Water pollution has become a serious problem for aquatic and human life as a result of industrialization because industries manufacture huge amounts of chemicals. Because of the rapid development of industry, a large percentage of industrial pollutants are thrown into the water without being properly handled. As a result, animals and plants in neighboring industrial regions have been severely threatened. Paper, ceramics, photography, printing, cosmetics, leather, and textiles have all dealt with a large number of dyes on a regular basis. These dyes are commonly employed as polymer-coating ingredients and as a colored substance. Yearly, 7×10^5 tons of different industrial pigments and dyes are created [2]. Among them, rose bengal (RB) is an organic (xanthene type) dye that is frequently used as a coloring material in dyeing industries, printing, and textiles. RB dye is described as cytostatic, cytotoxic, mutagenic, and genotoxic, and also obstructs leucine aminopeptidase [3].

However, polluted wastewater containing organic dyes causes numerous environmental problems as well as human health, thereby, demanding the development and execution

of a cost-effective and ecologically friendly remedy. Several research teams are attempting to cost-effectively solve environmental challenges concerning water resources. Ion exchange, chemical precipitation, coagulation, adsorption, electrolysis, and photocatalysis methods are generally used to remove the toxic contaminant from industrial wastewater [4]. However, the long-term viability of these traditional processes is still questionable due to the requirement of a huge volume of catalysts. Furthermore, such techniques have the potential to generate large volumes of secondary contaminants or to transfer one form to another. In terms of sustainability, the photocatalytic approach is very appropriate. Additionally, it is more suitable than others because of its low cost, superior performance, lack of secondary contaminant production, ease of operation, and environmental friendliness. In the photocatalysis system, hazardous pollutants are transformed into harmless products such as H_2O, CO_2, etc. with the help of reactive oxygen species [5–7]. Nevertheless, picking the right photocatalyst might be difficult.

Over the last decade, organic dyes have been removed from aqueous solutions using semiconductor metallic oxide nanoparticles, especially, SnO_2, $BiVO_4$, CeO_2, CuO, WO_3, TiO_2, Fe_2O_3, ZnO, etc. [1,8–15]. Among them, ZnO is widely used in various fields including photoluminescence emitters, electrode materials for energy storage, antibiotics, photocatalytic degradation of organic pollutants, etc. due to its nontoxicity, low price, good thermal conductor, environmentally stable nature, abundance in nature, and excellent optical and electrical properties [2,15,16]. However, the photocatalytic proficiency of the ZnO remains low due to the wide bandgap (3.37 eV), which increases the electron–hole (e^-–h^+) pairs recombination and reduces the photon consumption efficacy [14,17–19]. In addition, ZnO has very low photocatalytic activity under visible light and it can be used only using UV-light illumination with a wide bandgap. Therefore, it is currently a burning issue to enhance the photocatalytic efficiency of ZnO in visible-light irradiation by decreasing its bandgap energy.

Doping with metals or non-metals, mixing with other semiconductors, and fabricating nanoparticles have all been used to mitigate these drawbacks and improve the visible-light photocatalytic activity of pure ZnO [20]. Many research groups have described the photocatalytic efficiency of ZnO as being improved by metal doping elements compared to pure ZnO for the degradation of organic pollutants [21–24]. However, the catalytic activity of the metal-doped ZnO material did not reach a suitable level for practical implementation via visible-light irradiation. This is due to the doping metal ions that could perform as a e^-–h^+ pairs' recombination center, which decreases the catalytic activity [25,26]. In this respect, non-metal doping is the leading approach [16]. Therefore, non-metal nitrogen (N) has long been thought to be the best doping candidate because N and oxygen (O) have a similar ionic radius and N shows the lowest ionization energy among the group V elements [27]. The combination of O 2p and N 2p states decreases the semiconductor's bandgap, leading to increased absorption in the visible-light range [16]. In addition, the presence of N atom in the ZnO matrix can slow down the recombination of charge carriers, increase specific surface area, and speed up charge carrier transportation [28–31].

Motivated by the above hypothesis, herein, we prepared N-doped ZnO using the chemical vapor deposition (CVD) method to reduce the bandgap energy and enhance the photocatalytic efficiency of undoped ZnO in the visible-light illumination. RB dye was used as a model pollutant. To our knowledge, no one has reported on the degradation of RB dye either with UV light or visible light using N-doped ZnO. In addition, the as-synthesized N-doped ZnO compound was systematically studied and characterized by employing several spectroscopic and microscopic methods such as X-ray diffractometer (XRD), Fourier transform infrared (FTIR) spectroscopy, high-resolution field-emission scanning electron microscopy (HR-FE-SEM), energy-dispersive X-ray spectroscopy (EDS), HR-FE-SEM elemental mapping, UV–vis spectroscopy, and photoluminescence (PL) spectroscopy. The results confirmed that the successful preparation of N-doped ZnO and also indicated that the as-prepared sample was favorable for the deterioration of organic pollutants in the visible-light region. The photocatalytic activity, as well as reaction kinetics, were investi-

gated and found to have superior activity. Furthermore, the probable photodegradation mechanism of the RB dye using N-doped ZnO under visible light was proposed.

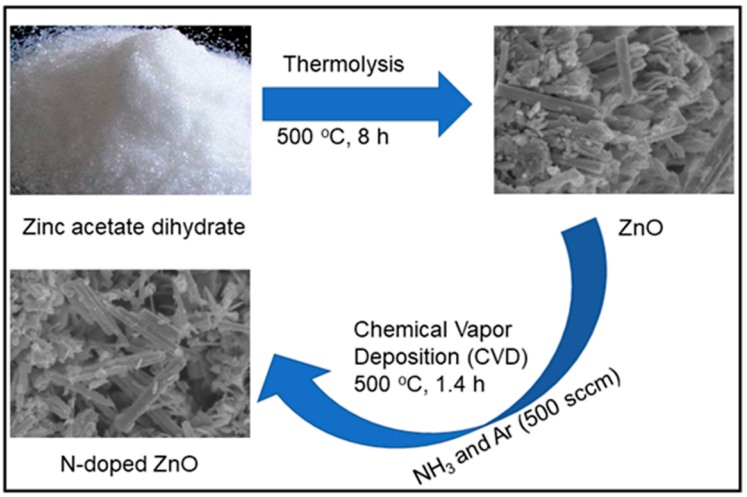
2. Materials and Methods

2.1. Materials

Zinc acetate dihydrate (99.0%) and RB dye were received from Sigma-Aldrich (St. Louis, MO, USA). Argon (99.99%) and ammonia (99.99%) gas were obtained from Hankook Special Gases Co., LTD (Iksan, Korea).

2.2. Synthesis of ZnO and N-Doped ZnO

Both the ZnO and N-doped ZnO were synthesized by the cost-effective facile techniques. At first, ZnO was prepared by a thermal process and then N was doped onto the as-prepared ZnO. In a typical experiment, 3 g of zinc acetate dihydrate was placed into a quartz crucible and capped with a lid to synthesize ZnO. The crucible was then sealed with an oxygen-free copper gasket in a stainless-steel chamber (SUS314; length = 60 mm, diameter = 35 mm). The compartment was positioned in a furnace (KSL-1100X-S-UL-LD, manufacturer, state, city, MTI Corporation, Richmond, CA, USA) and heated at 400 °C for 8 h with a 5 °C min^{-1} heat-up rate. For homogeneous and consistent production of ZnO material, the furnace was left undisturbed after thermolysis to cool gradually to an ambient temperature. Subsequently, N-doped ZnO was prepared followed by the chemical vapor deposition (CVD) method. In this case, an equal amount (500 sccm) of NH_3 and Ar gases flowed onto the as-synthesized ZnO at 500 °C temperature for 1.4 h. After that, the desired N-doped ZnO powder compound was collected and kept in a closed vial for further use. Scheme 1 shows the schematic diagram for the preparation of ZnO and N-doped ZnO.



Scheme 1. Schematic diagram for the preparation of ZnO and N-doped ZnO.

2.3. Characterization

The structural investigation was conducted by XRD (X'Pert PRO, PANalytical, Lelyweg, Almelo, The Netherlands) using Cu Kα radiation (λ = 1.5406 Å). FTIR (Thermo Fisher Scientific Nicolet iS5, Madison, WI, USA) was used to record typical bond vibrations in the as-prepared samples at an ambient temperature. The morphological analysis was carried out by HR-FE-SEM and Hitachi SU8230 was used for the HR-FE-SEM experiments. To examine the optical characteristics and calculate the bandgap energy values, a UV–vis spectrophotometer (Perkin Elmer Lambda 25, Ayer Rajah, Singapore) was employed. A spectrophotometer (FP-6500, Jasco, Tokyo, Japan) was used to measure PL.

2.4. Photocatalytic Experiments

As a targeted pollutant, RB dye degradation in the aqueous solution was used to assess the photocatalytic performance of undoped and N-doped ZnO samples. The experiments were carried out with a visible-light source of a halogen lamp (100 mW/cm^2). A 400 nm UV cut-off filter was also used to prevent UV exposure. A total of 100 mg of catalyst was disseminated in 100 mL of dye solution (10 ppm) in a typical experiment. After that, the suspension was magnetically stirred for 30 min to ensure dye molecule adsorption on the catalyst surface. This combination was then held in the dark environment for 30 min untouched condition to achieve adsorption–desorption equilibrium. After that, the photocatalytic degradation reaction was triggered by contact with the help of a light source. The mixture was constantly stirred to achieve uniformity of catalyst materials. The UV–vis absorption spectrum of the dye solution was recorded to track its deterioration. UV–vis spectrometry was used to capture absorbance values. Measurements were collected at different periods (0, 10, 20, 30, 40, 50, 60, 70, 80, 90, and 100 min) and a fixed amount of RB solution was taken for each test.

3. Results and Discussion

3.1. Structural Investigation

The crystal structure, phase, crystallite size, and purity of the ZnO and N-doped ZnO were investigated using XRD. Figure 1 reveals the XRD patterns of the examined samples in the range of 2θ = (15–80)°. The diffraction peaks of ZnO are centered at 2θ values of 31.43°, 34.12°, 35.98°, 47.29°, 56.36°, 62.61°, 66.18°, 67.71°, 68.87°, 72.38°, and 76.80°, and correspond to the (100), (002), (101), (102), (110), (103), (200), (112), (201), (004), and (202) planes, respectively, with hexagonal wurtzite ZnO structure (JCPDS #36-1451). All the XRD peaks of ZnO were observed in the curves of N-doped ZnO. In addition, after N-doping onto the ZnO, the most intense (101) plane was shifted toward higher 2θ values compared to ZnO alone (marked in Figure 1, dotted line). These outcomes suggest that N is doped onto the ZnO matrix. The XRD curve revealed no extra peaks were found due to N, indicating that the synthesized compound had not affected the crystal system of ZnO.

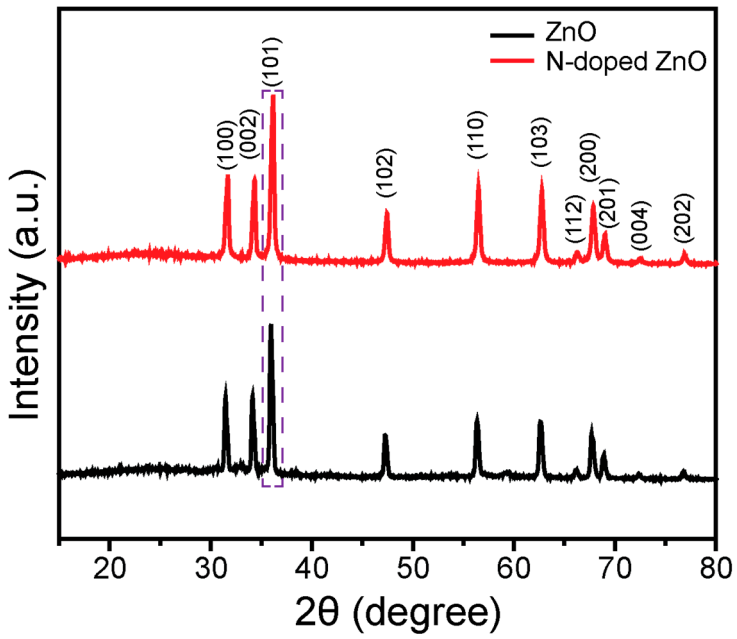


Figure 1. XRD patterns of the ZnO and N-doped ZnO.

The average crystallite size of the ZnO and N-doped ZnO (all the aforementioned planes) was evaluated employing Scherrer's Equation (1):

$$D = k\lambda/\beta\cos\theta \quad (1)$$

where D is the crystallite size, λ denotes an X-ray wavelength (0.15406), *k* refers to non-dimensional shape factor (0.94), θ signifies the Bragg angle, and β designates the full width at half maximum. The average D of the ZnO and N-doped ZnO was 23.96 and 21.94 nm, respectively. When compared to ZnO, N-doping caused significant peak broadening and reduction in crystallinity, which was attributable to a change in grain size. These findings showed that N was successfully integrated into the lattice of ZnO.

FTIR spectroscopy was applied to examine the functional groups and nature of the chemical bonding. The FTIR curves of ZnO and N-doped ZnO were investigated in the range of 400–4000 cm^{-1} and shown in Figure 2. The peak observed at 512 cm^{-1} was due to the stretching vibrational mode of ZnO. The ZnO hexagonal system was accountable for the peak centered between 400 and 555 cm^{-1} [32]. Interestingly, in N-doped ZnO, the peaks positioned at 1382 and 1509 cm^{-1} corresponded to the stretching mode of the N-Zn and N-Zn-O chemical bond, respectively. This finding supported the presence of an N atom in the ZnO crystalline structure [16]. Furthermore, both the compounds were assigned a wide peak between 3200 and 3600 cm^{-1} as a result of the stretching mode of surface-adsorbed O–H environment.

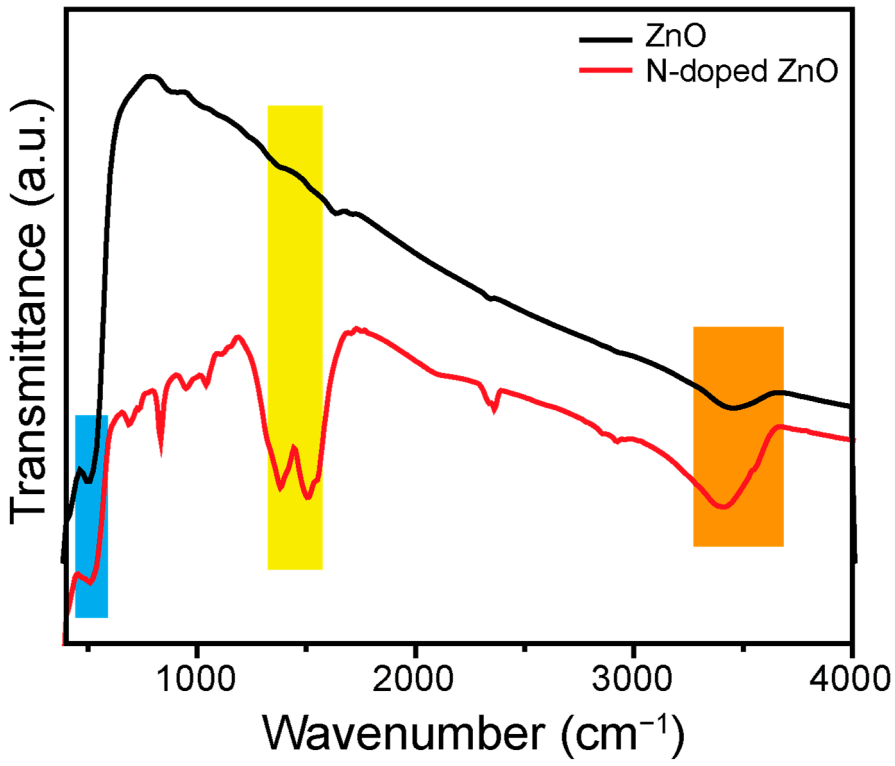


Figure 2. FTIR spectra of the ZnO and N-doped ZnO.

3.2. Morphological Investigation

One of the most important instruments for characterizing the surface morphology of the manufactured catalyst was HR-FE-SEM. Therefore, HR-FE-SEM was used to detect the morphological properties of ZnO and N-doped ZnO materials. Figure 3a shows the HR-FE-SEM micrograph of the as-prepared ZnO. These ZnO nanoparticles showed two types of morphological shapes: one was aggregated nearly spherical and the other one was rod-shaped. The gathering of tiny particles may be responsible for the production of aggregated nearly spherical shape nanoparticles. Most of the particles were of rod-like morphology and the average length and diameter were found to be approximately 3.3 μm and 450 nm, respectively. These rod-shaped ZnO nanoparticles followed a wurtzite hexagonal structure [33]. The results (wurtzite hexagonal structure) were in line with the results of the XRD analysis. Figure 3b reveals the N-doped ZnO nanoparticle's HR-FE-SEM micrograph. After the incorporation of N onto the ZnO, the morphological shape of the

particles remained intact, but the size was reduced. The average length and diameter of the N-doped samples were observed around 2.1 µm and 212 nm, respectively. These findings indicated that due to the doping of N, the axial growth of ZnO nanoparticles was suppressed. A similar outcome was identified for the doping of Mn onto ZnO nanorods [34]. This study demonstrated that the doping atom did not affect the particle's morphology.

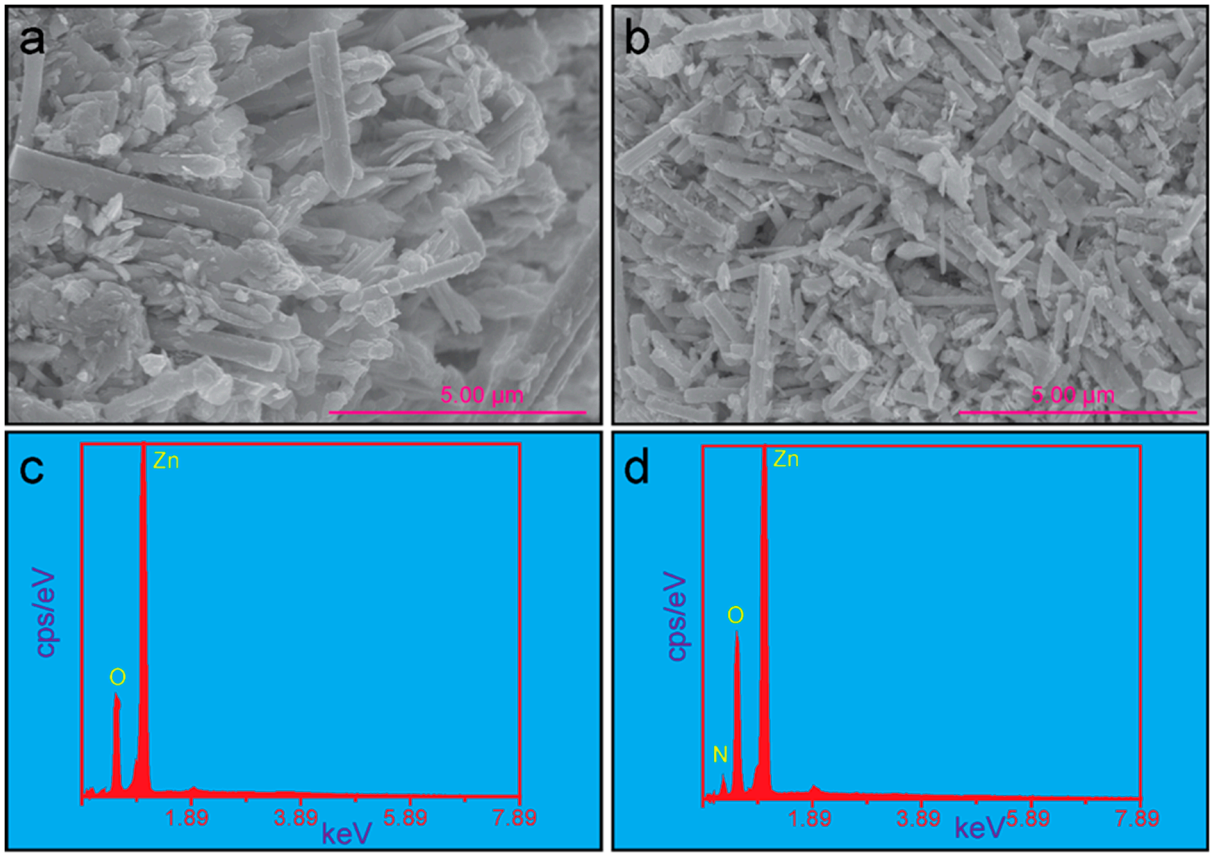


Figure 3. HR-FE-SEM images of (**a**) ZnO and (**b**) N-doped ZnO; ESD spectra of (**c**) ZnO and (**d**) N-doped ZnO.

In addition, the EDS experiment was evaluated to confirm the presence of elements and the purity of the as-synthesized compounds. Figure 3c displays the EDS spectrum of the ZnO. Only Zn and O elements were detected in the ZnO sample. Figure 3d shows three elements (N, Zn, and O) that were present in the N-doped ZnO material. These results further proved the successful formation of the N-doped ZnO compound. Moreover, both the as-prepared catalysts were highly pure due to the lack of extra peaks in the EDS spectra. The weight (wt.) and atomic (atm.) percentage of the ZnO and N-doped ZnO were shown in Table 1. The outcomes indicated that the N-doped ZnO sample was doped with a minor quantity of N. However, this small amount of N had a huge impact on the photocatalytic degradation of the pollutant (see Section 3.5) compared to undoped ZnO.

Furthermore, the elemental distribution of the N-doped ZnO was investigated using HR-FE-SEM elemental mapping analysis and is shown in Figure 4. The results showed that N-doped ZnO was composed of three elements (N, O, and Zn) and these three elements were uniformly distributed in the N-doped ZnO structure.

Table 1. Summary of analytical data for ZnO and N-doped ZnO.

Sample	Crystallite Size (Using Scherrer's Equation) (nm))	Particle Size (from HR-FE-SEM)		EDS Analysis			Bandgap (eV)
		Average Length (μm)	Average Diameter (nm)	Element	Weight %	Atomic %	
ZnO	23.96	3.3	450	Zn O	95.07 4.93	82.53 17.47	3.37
N-doped ZnO	21.94	2.1	212	N Zn O	0.19 96.40 3.41	0.78 86.69 12.53	3.32

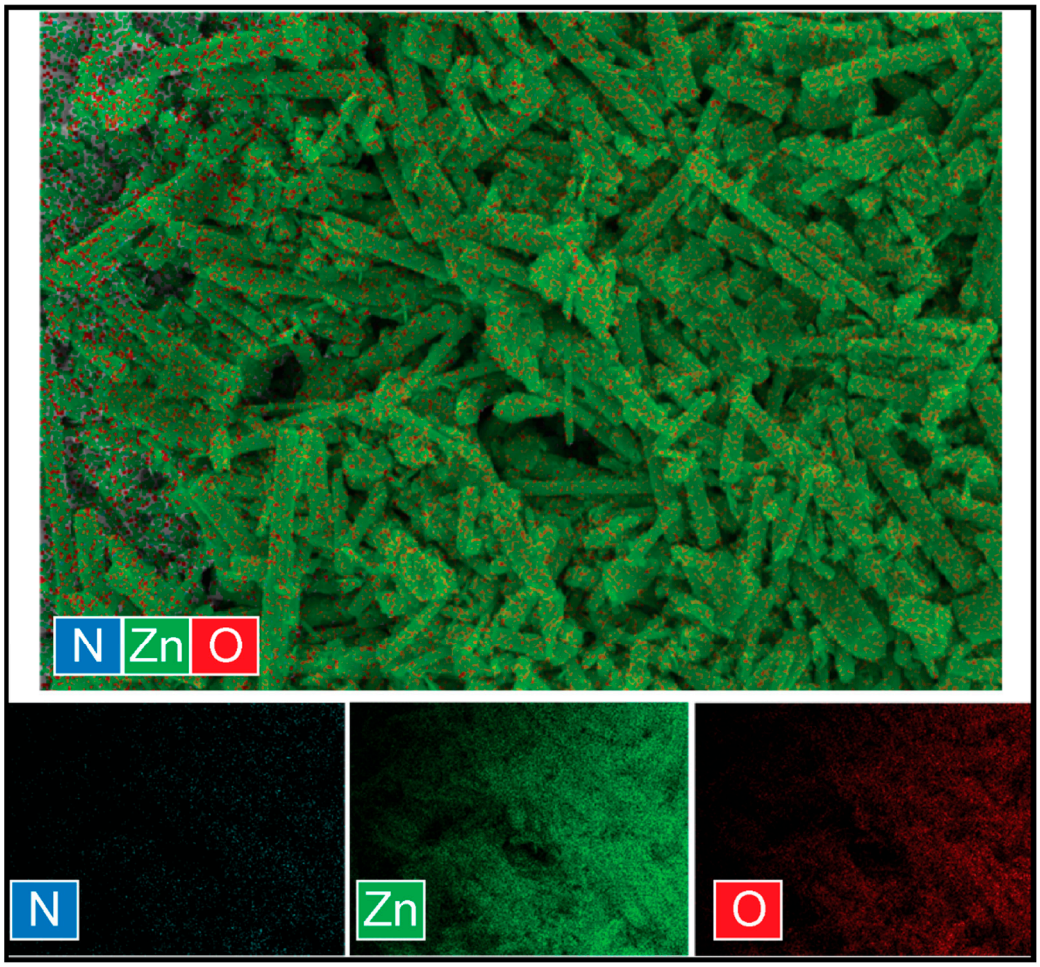


Figure 4. HR-FE-SEM elemental mapping investigation of N-doped ZnO.

3.3. Optical Investigation

The material's optical properties and bandgap energy (E_g) are critical features in its utilization as a photocatalyst. These characteristic properties of the ZnO and N-doped ZnO were determined using UV–vis spectroscopy. The as-prepared ZnO and N-doped ZnO materials were dispersed in an ethanol solution separately. Both the samples were kept at the same concentration (0.01 mg mL^{-1}), and their UV–vis absorbance was recorded. The UV–vis absorption spectra of the aforementioned compounds are shown in Figure 5a,b. The peaks at 368 and 373 nm corresponded to ZnO and N-doped ZnO, respectively. After the incorporation of N into ZnO, the absorption peak was shifted towards the visible region compared to the undoped ZnO. Thus, N-doped ZnO might show more comparatively enhanced photocatalytic activity in the visible region than for ZnO alone.

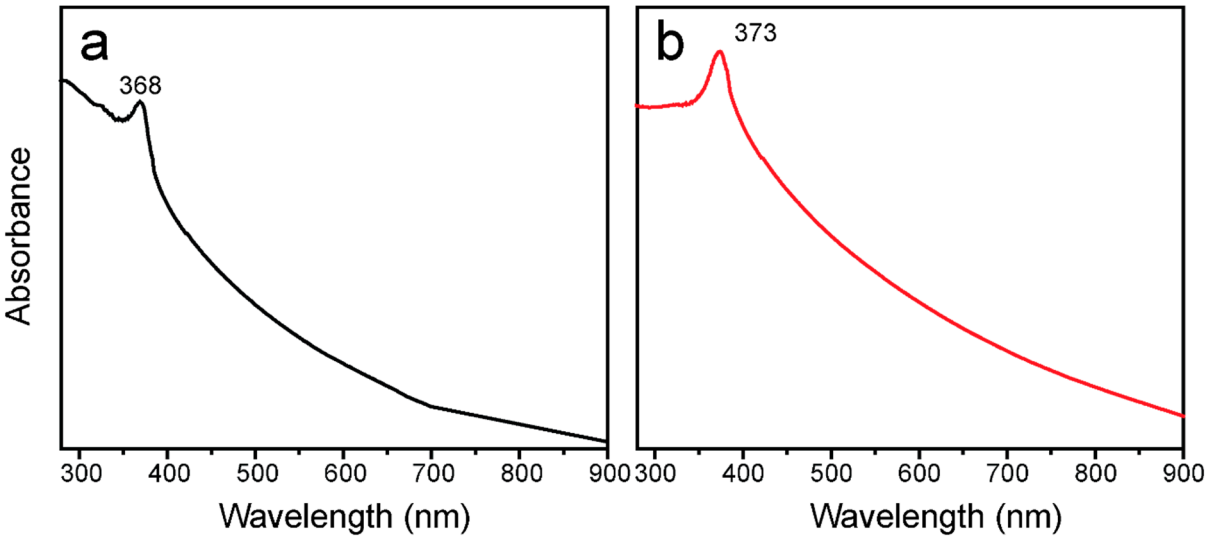


Figure 5. UV–vis absorption spectra of (**a**) ZnO and (**b**) N-doped ZnO.

Further, the E_g of the ZnO and N-doped ZnO was measured from the UV–vis absorption data by applying Planck's energy Equation (2):

$$E_g = \frac{hc}{\lambda} = \frac{1240}{\lambda}\ eV \quad (2)$$

where h is Plank's constant, c is the velocity of light, and λ is the wavelength of light. The estimated E_g value of the ZnO and N-doped ZnO was 3.37 and 3.32 eV, respectively. Surprisingly, after N-doped onto the ZnO material, the E_g value was reduced considerably than ZnO. The lower E_g value enhances the formation of e^-–h^+ pairs and reduced their recombination rate [32]. The photocatalytic efficiency of the semiconductor materials was enhanced due to the decreasing of E_g value. The investigated analytical data of ZnO and N-doped ZnO are summarized and shown in Table 1.

3.4. Photoluminescence (PL) Investigation

PL analysis was used to evaluate the charge carriers' recombination effect on the compounds. Figure 6 shows the PL spectra of the ZnO and N-doped ZnO using the excitation wavelength of 350 nm at room temperature. The peak of the samples was detected at a λ_{max} of approximately 472~477 nm. The PL intensity of the undoped ZnO was very high compared to N-doped ZnO. PL spectra were observed because of photon emission due to the recombination of e^-–h^+ pairs within the semiconductor material. The considerable reduction of PL intensity in the N-doped ZnO compound affirms the lower recombination effect of the photoinduced e^-–h^+ pairs, whereas the high-intensity peak of undoped ZnO refers to higher recombination of e^-–h^+ pairs. This means that N doping played a crucial role to suppress the e^-–h^+ pairs' recombination effect because the doping material created multiple electron traps that diminish the e^-–h^+ pairs recombination. The reduction of e^-–h^+ pairs' recombination increased the flow of electron transfer and separation, leading to an improvement of the the photocatalytic efficiency of the materials [35]. Therefore, this study suggests that N doping aided in the suppression of charge carriers' recombination, which might be advantageous for boosting photocatalytic proficiency.

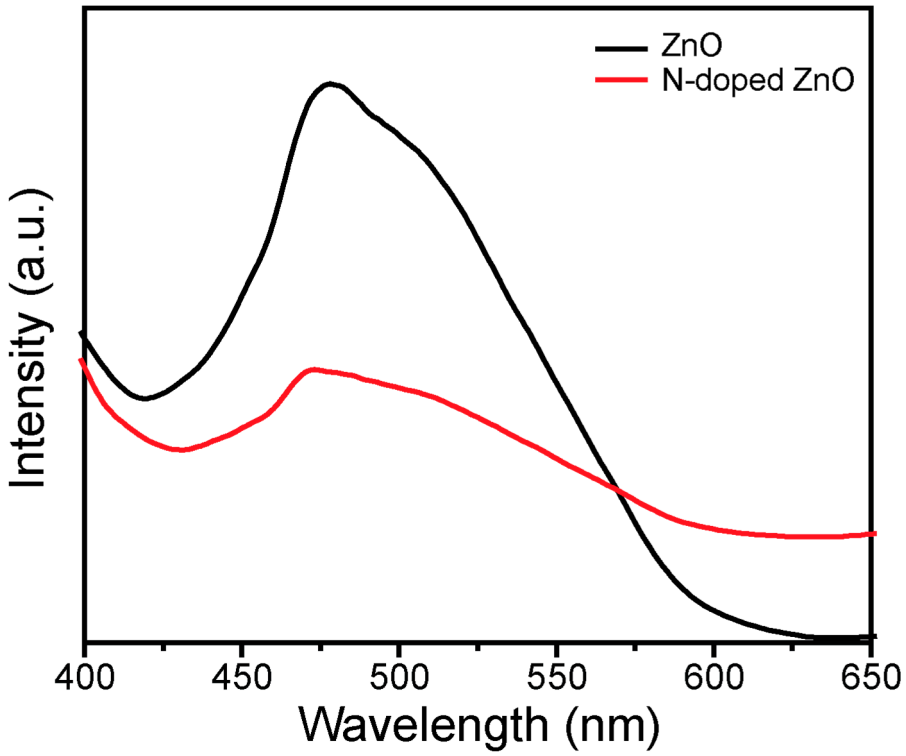


Figure 6. Photoluminescence spectra of ZnO and N-doped ZnO.

3.5. Photocatalytic Investigation

The photocatalytic behavior of the as-synthesized ZnO and N-doped ZnO was explored to degrade the toxic organic pollutant RB dye under visible-light irradiation. Figure 7 shows the observed photodegradation data as well as their kinetic plots. Figure 7a,b show the UV–vis absorbance spectra for the degradation of RB dye in the presence of ZnO and N-doped ZnO, respectively. Two representative absorption peaks arose at 549 and 511 nm corresponding to the monomer and dimer adsorption bands of RB dye, which were monitored for the evaluation of the photocatalytic efficiency. The intensities of both RB dye peaks significantly dropped as the irradiation period increased. In these cases, the degradation peaks of N-doped ZnO almost diminished compared to undoped ZnO within 100 min of visible-light illumination. In addition, the photographs of each inset before and after the photocatalytic reaction confirmed the deterioration performance of the samples by changing their corresponding color of RB dye.

The photocatalytic proficiency (η) of the as-constructed ZnO and N-doped ZnO catalyst was measured using the following Equation (3) [36]:

$$\eta\ (\%) = \frac{C_0 - C_t}{C_0} \times 100 \quad (3)$$

where C_t represents the absorbance at the time (t) min and C_0 refers to the absorbance at the time 0 min. Figure 7c displays the photocatalytic proficiency of ZnO and N-doped ZnO. The calculated efficiency of the ZnO and N-doped ZnO photocatalyst was found to be 62.95 and 96.90%, respectively, after 100 min of visible-light irradiation. Surprisingly, up to 40 min, the degradation efficiency was almost 53 and 65% for ZnO and N-doped ZnO, respectively. After that, the photocatalytic activity of N-doped ZnO was regularly increased, whereas ZnO was very slowly degrading the RB dye. This was because in the undoped ZnO, the e^-–h^+ pairs' recombination effect enhanced and thereby suppressed the degradation activity. Interestingly, the targeted N-doped ZnO material confirmed the maximum efficiency (96.90%) and was observed 154% higher than undoped ZnO. The results indicated that the photodeterioration performance of ZnO was considerably

enhanced after the introduction of N onto the ZnO matrix. The optical properties, i.e., absorption of light efficiency of ZnO was enhanced due to the doping of N onto the ZnO system. As a result, the flow of electrons was increased and the recombination of e^-–h^+ pairs diminished, which boosted the photocatalytic activity of the N-doped ZnO.

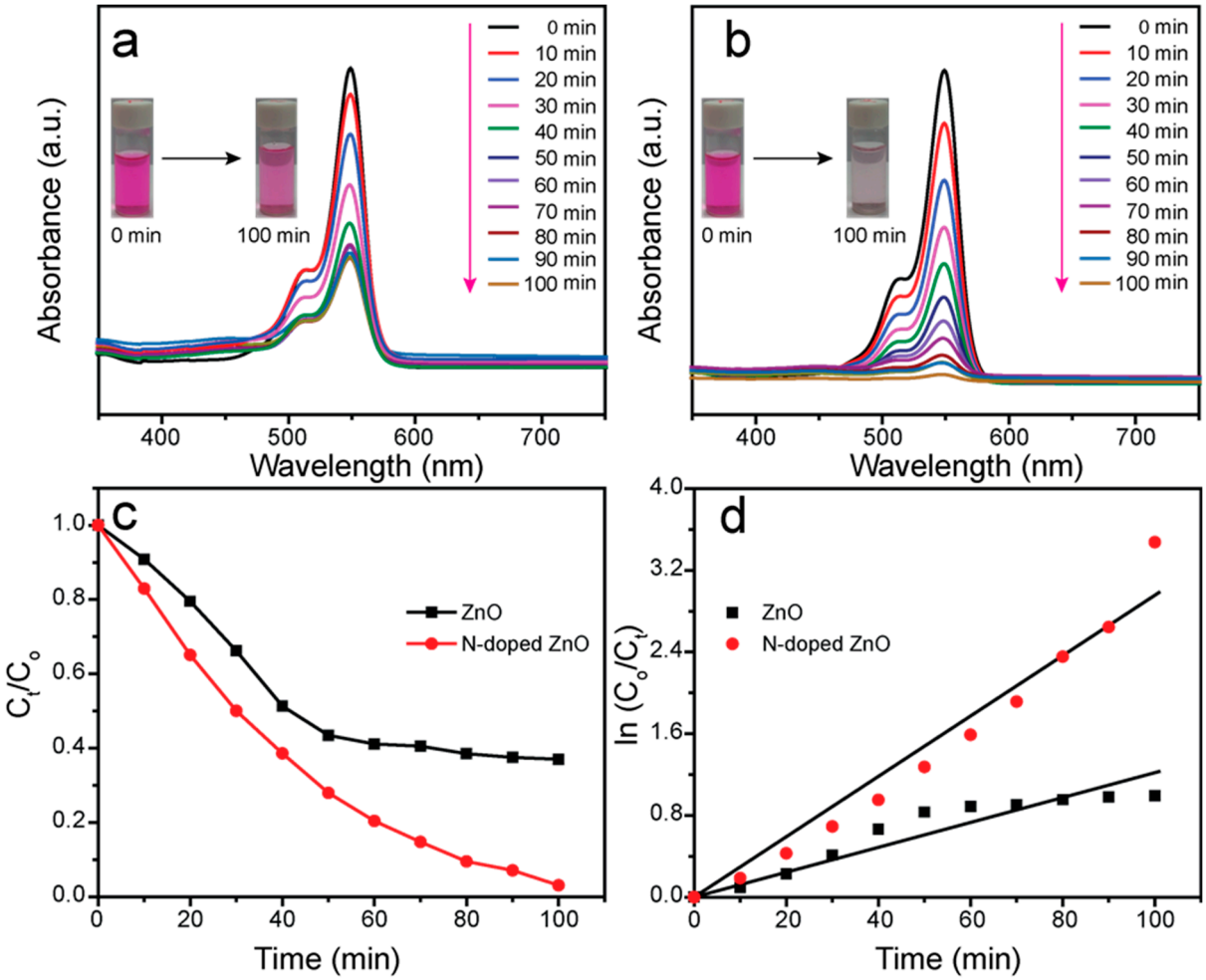


Figure 7. UV–vis absorbance spectra for the decomposition of RB dye in the presence of (**a**) ZnO and (**b**) N-doped ZnO (each inset shows the color variation of RB dye before (0 min) and after (100 min) photocatalytic reaction); (**c**) photodegradation activity as a function of time (**d**) and their corresponding kinetics.

A reaction kinetics investigation of the ZnO and N-doped ZnO compounds was also carried out in order to better understand the catalytic efficiency and their corresponding results displayed in Figure 7d. A pseudo-first-order reaction kinetics equation was applied to determine the RB dye degradation rate constant and this Equation (4) is given below:

$$\ln\left(\frac{C_0}{C_t}\right) = kt \quad (4)$$

where k and t are called rate constant and the reaction irradiation time, respectively. The calculated k value of undoped ZnO and N-doped ZnO were 0.01 and 0.03 min^{-1}, respectively. The k value of N-doped ZnO was three times higher compared to undoped ZnO. These outcomes clearly indicated that the improvement of photocatalytic proficiency was due to the introduction of N onto ZnO. Therefore, the doping element had a dynamic role in improving photodegradation proficiency as well as rate constant compared to the undoped material.

The photocatalytic activity of the N-doped ZnO material was compared to that of the previously published ZnO-containing compound, as shown in Table 2. The N-doped ZnO performed well in terms of degradation efficiency and time when compared with others.

Table 2. A comparison of the photocatalytic degradation performance of various ZnO-containing photocatalysts.

Photocatalyst	Pollutant (Dye)	Light Source	Degradation (%)	Time (min)	Ref.
Cu/ZnO	DB [1] 15	Visible light	70	120	[21]
Sr/ZnO	MB [2]	Visible light	50	120	[22]
La/ZnO	MO [3]	Visible light	85.8	150	[23]
Sn/ZnO	MB	Visible light	81	120	[24]
ZnS NRs [4]	RB	Visible light	93	225	[37]
N-ZnO	MB	Visible light	98	120	[38]
[5] RGO-N-ZnO	MB	Visible light	98.5	120	[39]
N-ZnO/C-dots	MG [6]	Visible light	85	160	[13]
N-doped ZnO	RB	Visible light	96.90	100	This work

[1] DB = direct blue, [2] MB = methylene blue, [3] MO = methyl orange, [4] NRs = nanorods, [5] RGO = reduced graphene oxide, [6] MG = malachite green.

3.6. Photocatalytic Mechanism

The plausible photocatalytic degradation mechanism of RB dye in the presence of the N-doped ZnO catalyst is illustrated in Figure 8. Based on the UV–vis data, the wavelength range and E_g value were both beneficial for the degradation of organic contaminants when exposed to visible light. Furthermore, the PL results indicated that e^-–h^+ pair recombination was inhibited once N was included in the ZnO material. The photoinduced holes (h^+) and electrons (e^-) were created on the interface of the N-doped ZnO compound when it was contacted by light illumination (Equation (5)). The conduction band (CB) transport3e e^-, whereas the valence band (VB) stores h^+. The e^-s acted as a reductant, whereas the h^+s performed as an oxidant. In the VB, h^+ reacted with H_2O to produce hydroxyl radicals ($HO^\bullet$, Equation (6)). At the same time, superoxide radicals ($O_2{}^{-\bullet}$) were generated in the CB by reacting with oxygen molecules and e^- (Equation (7)). The generated $O_2{}^{-\bullet}$ radicals further help to create $HO^\bullet$ radicals, including several reactions (Equations (8)–(12)). Finally, the RB dye was degraded with the assistance of the produced $HO^\bullet$ radicals (Equation (13)). The overall photodegradation reaction mechanism is given below:

$$h\nu + \text{N-doped ZnO} \rightarrow \text{N-doped ZnO } (h^+{}_{VB} + e^-{}_{CB}) \quad (5)$$

$$H_2O + h^+{}_{VB} \rightarrow HO^\bullet + H^+ \quad (6)$$

$$O_2 + e^-{}_{CB} \rightarrow O_2{}^{-\bullet} \quad (7)$$

$$O_2{}^{-\bullet} + H^+ \rightarrow HO_2{}^\bullet \quad (8)$$

$$HO_2{}^\bullet + HO_2{}^\bullet \rightarrow H_2O_2 + O_2 \quad (9)$$

$$H_2O_2 + O_2{}^{-\bullet} \rightarrow O_2 + HO^- + HO^\bullet \quad (10)$$

$$h\nu + H_2O_2 \rightarrow 2HO^\bullet \quad (11)$$

$$e^- + H_2O_2 \rightarrow HO^- + HO^\bullet \quad (12)$$

$$\text{RB dye} + (HO^\bullet, O_2{}^{-\bullet}) \rightarrow \text{Degradation products} \quad (13)$$

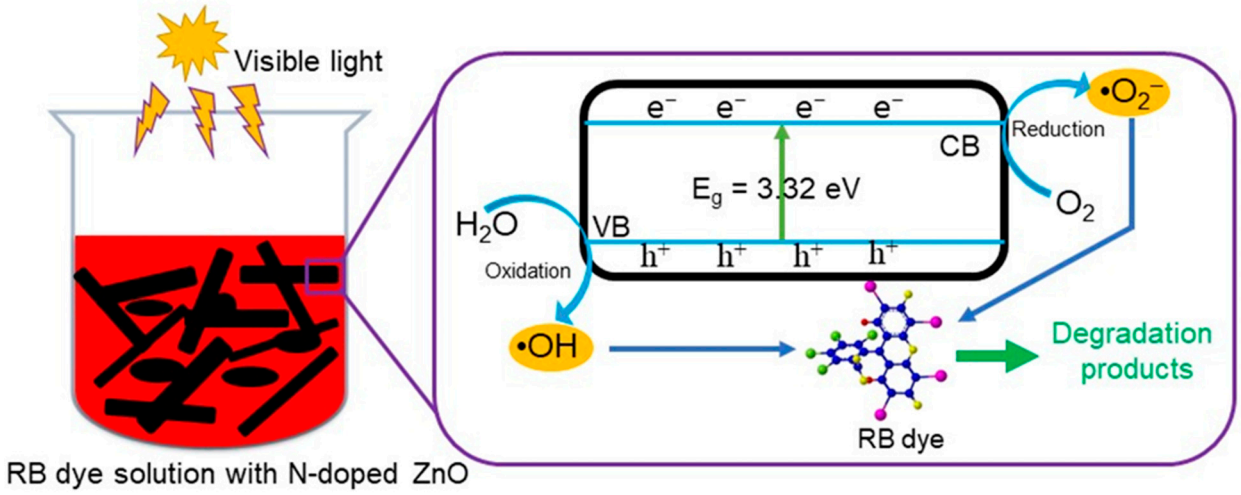


Figure 8. The proposed photocatalytic mechanism for the degradation of RB dye using N-doped ZnO catalyst.

4. Conclusions

We used a simple chemical vapor deposition process to synthesize N-doped ZnO, which was applied to degrade wastewater containing toxic RB dye under visible exposure. Various spectroscopic and microscopic approaches were employed to investigate the as-prepared N-doped ZnO and the undoped ZnO. The XRD and FTIR analyses confirmed that the as-prepared samples were hexagonal structures, and due to the N doping, had no effect on the structure of ZnO crystal. The HR-FE-SEM outcomes indicated the average length and diameter of the N-doped samples were noticeably reduced than undoped ZnO. The as-synthesized product was free from impurities. It contained only N, Zn, and O elements according to EDS and elemental mapping analysis. The absorption peak extended into the visible range and the E_g value decreased sharply compared to the control sample, which increased the electron flow and diminished the e^-–h^+ pair recombination. In addition, the UV–vis and PL results showed N-doped ZnO could be a suitable candidate for photocatalysts. Within 100 min of visible-light illumination, the RB dye photodegradation efficiency of the doped sample was 154% higher than undoped ZnO. The rate constant was also three times higher compared to undoped ZnO. Therefore, it was clearly proven that N played a crucial role in these improvements. These findings provide an encouraging pathway for developing excellent and enhanced N-doped photocatalysts.

Author Contributions: Conceptualization, M.A.H.; Methodology, M.A.H.; Software, M.A.H.; Formal analysis, M.A.H., Y.S.K. and S.A.; Investigation, M.A.H.; Data curation, M.A.H., Y.S.K. and S.A.; Writing—original draft preparation, M.A.H.; Writing—review and editing, M.A.H., Y.S.K., S.A., H.G.K. and L.K.K.; Visualization, H.G.K. and L.K.K.; Supervision, L.K.K.; Project administration, L.K.K.; Funding acquisition, L.K.K. All authors have read and agreed to the published version of the manuscript.

Funding: This research was supported by the Basic Science Research Program through the National Research Foundation of Korea (NRF) funded by the Ministry of Education (2016R1A6A1A03012069, 2018R1D1A1B07050752).

Institutional Review Board Statement: Not applicable.

Informed Consent Statement: Not applicable.

Data Availability Statement: Not applicable.

Conflicts of Interest: The authors declare no conflict of interest.

References

1. Akter, J.; Sapkota, K.P.; Hanif, M.A.; Islam, M.A.; Abbas, H.G.; Hahn, J.R. Kinetically controlled selective synthesis of Cu_2O and CuO nanoparticles toward enhanced degradation of methylene blue using ultraviolet and sun light. *Mater. Sci. Semicond. Process.* **2021**, *123*, 105570. [CrossRef]
2. Hanif, M.A.; Akter, J.; Lee, I.; Islam, M.A.; Sapkota, K.P.; Abbas, H.G.; Hahn, J.R. Formation of chemical heterojunctions between ZnO nanoparticles and single-walled carbon nanotubes for synergistic enhancement of photocatalytic activity. *J. Photochem. Photobiol. A Chem.* **2021**, *413*, 113260. [CrossRef]
3. Japinder, K.; Sonal, S. Heterogeneous photocatalytic degradation of rose bengal: Effect of operational parameters. *Phys. B* **2014**, *450*, 49–53.
4. Akter, J.; Hanif, M.A.; Islam, M.A.; Sapkota, K.P.; Hahn, J.R. Selective growth of Ti^{3+}/TiO_2/CNT and Ti^{3+}/TiO_2/C nanocomposite for enhanced visible-light utilization to degrade organic pollutants by lowering TiO_2-bandgap. *Sci. Rep.* **2021**, *11*, 9490. [CrossRef]
5. Natarajan, S.; Bajaj, H.C.; Tayade, R.J. Recent advances based on the synergetic effect of adsorption for removal of dyes from waste water using photocatalytic process. *J. Environ. Sci.* **2018**, *65*, 201–222. [CrossRef] [PubMed]
6. Crini, G.; Lichtfouse, E. Advantages and disadvantages of techniques used for wastewater treatment. *Environ. Chem. Lett.* **2019**, *17*, 145–155. [CrossRef]
7. Vivek, E.; Senthilkumar, N.; Pramothkumar, A.; Vimalan, M.; Potheher, I.V. Synthesis of flower-like copper oxide microstructure and its photocatalytic property. *Phys. B Condens. Matter* **2019**, *566*, 96–102. [CrossRef]
8. Linhua, X.; Yang, Z.; Zijun, W.; Gaige, Z.; Jiaojiao, H.; Yanjing, Z. Improved photocatalytic activity of nanocrystalline ZnO by coupling with CuO. *J. Phys. Chem. Solids* **2017**, *106*, 29–36.
9. Sabzehmeidani, M.M.; Karimi, H.; Ghaedi, M. Enhanced visible light-active CeO_2/CuO/Ag_2CrO_4 ternary heterostructures based on CeO_2/CuO nanofber heterojunctions for the simultaneous degradation of a binary mixture of dyes. *New J. Chem.* **2020**, *44*, 5033–5048. [CrossRef]
10. Su, J.; Guo, L.; Bao, N.; Grimes, C.A. Nanostructured WO_3/$BiVO_4$ heterojunction flms for efficient photoelectrochemical water splitting. *Nano Lett.* **2011**, *11*, 1928–1933. [CrossRef] [PubMed]
11. Chen, X.; Wu, Z.; Liu, D.; Gao, Z. Preparation of ZnO photocatalyst for the efficient and rapid photocatalytic degradation of azo dyes. *Nanoscale Res. Lett.* **2017**, *12*, 143–152. [CrossRef] [PubMed]
12. Kumar, M.P.; Josephine, G.A.S.; Sivasamy, A. Oxidation of organic dye using nanocrystalline rare earth metal ion doped CeO_2 under UV and visible light irradiations. *J. Mol. Liq.* **2017**, *242*, 789–797. [CrossRef]
13. Sharma, S.; Mehta, S.K.; Kansal, S.K. N doped ZnO/C-dots nanoflowers as visible light driven photocatalyst for the degradation of malachite green dye in aqueous phase. *J. Alloys Compd.* **2017**, *699*, 323–333. [CrossRef]
14. Kumar, S.G.; Rao, K.S.R.K. Comparison of modification strategies towards enhanced charge carrier separation and photocatalytic degradation activity of metal oxide semiconductors (TiO_2, WO_3 and ZnO). *Appl. Surf. Sci.* **2016**, *391*, 124–148. [CrossRef]
15. Hanif, M.A.; Lee, I.; Akter, J.; Islam, M.A.; Zahid, A.A.S.M.; Sapkota, K.P.; Hahn, J.R. Enhanced photocatalytic and antibacterial performance of ZnO nanoparticles prepared by an efficient thermolysis method. *Catalysts* **2019**, *9*, 608. [CrossRef]
16. Hamdah, S.A.; Naushad, A.; Fahad, A.A. Synthesis of Gd/N co-doped ZnO for enhanced UV-vis and direct solar-light-driven photocatalytic degradation. *RSC Adv.* **2021**, *11*, 10194.
17. Wang, M.; Zhang, Y.; Zhou, Y.; Yang, F.; Kim, E.J.; Hahn, S.H.; Seong, S.G. Rapid room-temperature synthesis of nanosheet-assembled ZnO mesocrystals with excellent photocatalytic activity. *CrystEngComm* **2013**, *15*, 754–763. [CrossRef]
18. Habib, A.; Shahadat, T.; Bahadur, N.M.; Ismail, I.M.I.; Mahmood, A.J. Synthesis and characterization of ZnO-TiO_2 nanocomposites and their application as photocatalysts. *Int. Nano Lett.* **2013**, *3*, 5. [CrossRef]
19. Dindar, B.; Içli, S. Unusual photoreactivity of zinc oxide irradiated by concentrated sunlight. *J. Photochem. Photobiol. A Chem.* **2001**, *140*, 263–268. [CrossRef]
20. Lavand, A.B.; Malghe, Y.S. Synthesis, characterization and visible light photocatalytic activity of nitrogen-doped zinc oxide nanospheres. *J. Asian Ceram. Soc.* **2015**, *3*, 305–310. [CrossRef]
21. Ebrahimi, R.; Hossienzadeh, K.; Maleki, A.; Ghanbari, R.; Rezaee, R.; Safari, M.; Shahmoradi, B.; Daraei, H.; Jafari, A.; Yetilmezsoy, K. Effects of doping zinc oxide nanoparticles with transition metals (Ag, Cu, Mn) on photocatalytic degradation of Direct Blue 15 dye under UV and visible light irradiation. *J. Environ. Health Sci. Eng.* **2019**, *17*, 479–492. [CrossRef]
22. Yousefi, R.; Jamali-Sheini, F.; Cheraghizade, M.; Khosravi-Gandomani, S.; Saáaedi, A.; Huang, N.M.; Basirun, W.J.; Azarang, M. Enhanced visible-light photocatalytic activity of strontium-doped zinc oxide nanoparticles. *Mater. Sci. Semicond. Process.* **2015**, *32*, 152–159. [CrossRef]
23. Nguyen, L.T.; Nguyen, L.T.; Duong, A.T.; Nguyen, B.D.; Hai, N.Q.; Chu, V.H.; Nguyen, T.D.; Bach, L.G. Preparation, characterization and photocatalytic activity of La-doped zinc oxide nanoparticles. *Materials* **2019**, *12*, 1195. [CrossRef]
24. Arshad, M.; Qayyum, A.; Abbas, G.; Haider, R.; Iqbal, M.; Nazir, A. Influence of different solvents on portrayal and photocatalytic activity of tin-doped zinc oxide nanoparticles. *J. Mol. Liq.* **2018**, *260*, 272–278. [CrossRef]
25. Hofmann, M.R.; Martin, S.T.; Choi, W.; Bahnemann, D.W. Environmental applications of semiconductor photocatalysis. *Chem. Rev.* **1995**, *95*, 69–96. [CrossRef]
26. Anpo, M.; Takeuchi, M. The design and development of highly reactive titanium oxide photocatalysts operating under visible light irradiation. *J. Catal.* **2003**, *216*, 505–516. [CrossRef]

27. Qin, H.; Li, W.; Xia, Y.; He, T. Photocatalytic activity of heterostructures based on ZnO and N-doped ZnO. *ACS Appl. Mater. Interfaces* **2011**, *3*, 3152–3156. [CrossRef]
28. Palanivel, B.; Mani, A. Conversion of a type-II to a Z scheme heterojunction by intercalation of a 0D electron mediator between the integrative $NiFe_2O_4$/g-C_3N_4 composite nanoparticles: Boosting the radical production for photo-fenton degradation. *ACS Omega* **2020**, *5*, 19747–19759. [CrossRef]
29. Palanivel, B.; Shkir, M.; Alshahrani, T.; Mani, A. Novel $NiFe_2O_4$ deposited S-doped g-C_3N_4 nanorod: Visible-light driven heterojunction for photo-Fenton like tetracycline degradation. *Diam. Relat. Mater.* **2020**, *112*, 108148. [CrossRef]
30. Dhonde, M.; Sahu, K.; Murty, V.V.S.; Nemala, S.S.; Bhargava, P.; Mallick, S. Enhanced photovoltaic performance of a dye sensitized solar cell with Cu/N Codoped TiO_2 nanoparticles. *J. Mater. Sci. Mater. Electron.* **2018**, *29*, 6274–6282. [CrossRef]
31. Gupta, R.; Eswar, N.K.R.; Modak, J.M.; Madras, G. Visible light driven efficient N and Cu co-doped ZnO for photoinactivation of Escherichia coli. *RSC Adv.* **2016**, *6*, 85675–85687. [CrossRef]
32. Hanif, M.A.; Akter, J.; Kim, Y.S.; Kim, H.G.; Hahn, J.R.; Kwac, L.K. Highly efficient and sustainable ZnO/CuO/g-C_3N_4 photocatalyst for wastewater treatment under visible light through heterojunction development. *Catalysts* **2022**, *12*, 151. [CrossRef]
33. Buryi, M.; Remeš, Z.; Babin, V.; Novotný, M.; Vaněček, V.; Dragounová, K.A.; Mičová, J.; Landová, L.; Kučerková, R.; More-Chevalier, J.; et al. Influence of Mo doping on the luminescence properties and defect states in ZnO nanorods. Comparison with ZnO: Mo thin films. *Appl. Surf. Sci.* **2021**, *555*, 149679. [CrossRef]
34. Jing, L.; Zhihui, D.; Hongbo, L. Controllable Mn-doped ZnO nanorods for direct assembly of a photoelectrochemical aptasensor. *Analyst* **2017**, *142*, 2177.
35. Hanif, M.A.; Akter, J.; Islam, M.A.; Sapkota, K.P.; Hahn, J.R. Visible-light-driven enhanced photocatalytic performance using cadmium-doping of tungsten (VI) oxide and nanocomposite formation with graphitic carbon nitride disks. *Appl. Surf. Sci.* **2021**, *565*, 150541. [CrossRef]
36. Akter, J.; Hanif, M.A.; Islam, M.A.; Sapkota, K.P.; Lee, I.; Hahn, J.R. Visible-light-active novel α-Fe_2O_3/Ta_3N_5 photocatalyst designed by band-edge tuning and interfacial charge transfer for effective treatment of hazardous pollutants. *J. Environ. Chem. Eng.* **2021**, *9*, 106831. [CrossRef]
37. Maji, S.K.; Dutta, A.K.; Srivastava, D.N.; Paul, P.; Mondal, A.; Adhikary, B. Effective photocatalytic degradation of organic pollutant by ZnS nanocrystals synthesized via thermal decomposition of single-source precursor. *Polyhedron* **2011**, *30*, 2493. [CrossRef]
38. Sudrajat, H.; Babel, S. Photocatalytic degradation of methylene blue using visible light active N-doped ZnO. *Adv. Mater. Res.* **2015**, *1101*, 299–302. [CrossRef]
39. Suresh, M.; Sivasamy, A. Fabrication of graphene nanosheets decorated by nitrogen-doped ZnO nanoparticles with enhanced visible photocatalytic activity for the degradation of Methylene Blue dye. *J. Mol. Liq.* **2020**, *317*, 114112. [CrossRef]